



Effect of pressure on counterflow H₂–air partially premixed flames

Alejandro Briones, Ishwar K. Puri¹, Suresh K. Aggarwal^{*}

University of Illinois at Chicago, Department of Mechanical and Industrial Engineering, 842 West Taylor Street, Chicago, IL 60607, USA

Received 28 April 2004; received in revised form 15 September 2004; accepted 14 October 2004

Available online 23 November 2004

Abstract

A computational investigation of high-pressure hydrogen–air partially premixed flames (PPFs) is reported to characterize the effect of pressure on the flame structure, and the relevance of reaction limits for these flames. The flames are computed using the Mueller mechanism consisting of 19 elementary reactions and 9 species. Although the mechanism has been validated during previous investigations, additional validations are provided at high pressure. The PPF structure is characterized by two spatially distinct reaction zones, namely a rich premixed zone on the fuel side and a nonpremixed zone on the air side. In both reaction zones, consumption of reactants occurs primarily through reactions $\text{H} + \text{O}_2 \leftrightarrow \text{OH} + \text{O}$ (R1), $\text{H}_2 + \text{O} \leftrightarrow \text{OH} + \text{H}$ (R2), $\text{H}_2 + \text{OH} \leftrightarrow \text{H}_2\text{O} + \text{H}$ (R3), and $\text{H} + \text{O}_2 + \text{M} \leftrightarrow \text{HO}_2 + \text{M}$ (R9). As pressure increases, it decreases the physical separation between the two reaction zones. This can be attributed to the effects of pressure on (i) flame speed associated with the rich premixed zone, which moves this zone further downstream and (ii) mass diffusivity which moves the nonpremixed zone further upstream (toward the fuel nozzle). At higher pressures, however, these effects are significantly reduced, and the flame maintains its twin-flame structure even at very high pressures. Three reaction limits are identified for these flames. While the chemical structure of the nonpremixed zone is characterized by the first reaction limit in the range of pressure investigated ($p = 1$ to 40 atm), that of the rich premixed zone is characterized by transition from first to second limit, and then from second to third limit, as pressure is increased. This implies that H₂–air PPFs can exploit the advantages of the two reaction zones; each dominated by different reaction limits or chain reactions. Thermal radiation is found to have a negligible effect on the flame structure, while the Soret effect is found to cause transition between the reaction limits at lower pressure.

© 2004 The Combustion Institute. Published by Elsevier Inc. All rights reserved.

Keywords: Hydrogen partially premixed flames; Pressure effects; Reaction limits; Soret effect

1. Introduction

Partially premixed flames (PPFs) are established when less than a stoichiometric amount of oxidizer is mixed with the fuel stream before it enters the reaction zone, where additional air is available for complete combustion. These flames contain multiple (e.g.,

^{*} Corresponding author. Fax: +1-312-413-0441.

E-mail address: ska@uic.edu (S.K. Aggarwal).

¹ Current address: Virginia Tech, Blacksburg, VA, USA.

two or more) reaction zones and their overall structure is determined by the interactions between these zones. PPFs occur widely in practical combustion systems either by design or inadvertently due to poor mixing, spray vaporization [1], flame liftoff [2], and local extinction followed by reignition in turbulent flames [3]. For example, the combustion processes in spark-ignition [1] and diesel [4] engines are dominated by partially premixed combustion at elevated pressures.

There is growing interest in the use of hydrogen fuels for transportation and power generation. When burning in air, hydrogen has a larger energy release per unit mass (about 2.6 times that of gasoline), superior ignition characteristics, and significantly wider flammability limits compared to hydrocarbon fuels. Our literature survey of previous experimental work on hydrogen flames is presented in Table 1. Outwardly propagating spherical flames have been used to relate flame speed to stretch, but not to study the flame structure. Counterflow premixed and non-premixed configurations have been used to investigate the ignition of H_2 – O_2 chemistry. The table reports only one experimental study related to partially premixed flames, which is at atmospheric pressure.

Most past experiments concerning hydrogen combustion have been conducted by diluting hydrogen with He, Ar, or N_2 . However, practical applications generally involve partially premixed flames that are established by burning hydrogen in air. In the absence of fundamental investigations of hydrogen/air PPFs, the present study is relevant for understanding the flame structure and behavior of these flames at high pressures. Numerous efforts are underway focusing on the use of hydrogen in fuel cells and hydrogen-based IC engines [5–7]. Al-Baghdadi [8], Choudhuri and Gollahalli [9], and Kumar et al. [10] have shown that using blends of hydrogen and hydrocarbon fuels can improve both the emissions characteristics and the performance of combustors.

There are significant fundamental differences between the structures of hydrocarbon/air and hydrogen/air PPFs. Moreover, the literature contains no references to the effects of pressure on PPFs, although combustion in most applications, such as diesel engines and gas turbine combustors, occurs at high pressures and predominantly in a partially premixed mode. Our literature review, which is summarized in Table 1, indicates only two previous investigations of H_2 /air PPFs, both of which were conducted at atmospheric pressure. One of these considered the effects of diluents on NO_x emissions from a counterflow H_2 /air PPF [11], whereas the other investigated the propagation characteristics of a triple flame in a H_2 /air mixing layer [12,13]. In contrast, the effect of pressure on diluted hydrogen counterflow non-

premixed flames has been extensively investigated to examine ignition [14–16] and extinction characteristics [17]. Pressure effects on rich premixed hydrogen/air flames have also been characterized [18].

In a recent investigation [19] we demonstrated that for H_2 /air PPFs the fuel is only partially consumed in the rich premixed zone, with the remainder being transported and consumed in the nonpremixed zone. Consequently, the fuel oxidation chemistry in the two reaction zones and interactions between them are significantly different for H_2 /air PPFs compared to those for hydrocarbon/air PPFs. In both reaction zones, consumption of the reactants occurs primarily through reactions $H + O_2 \leftrightarrow OH + O$ (R1), $H_2 + O \leftrightarrow OH + H$ (R2), $H_2 + OH \leftrightarrow H_2O + H$ (R3), and $H + O_2 + M \leftrightarrow HO_2 + M$ (R9). Because both reaction zones are dominated by the pressure-dependent reaction (R9), pressure variations can be expected to significantly influence the flame structure. In particular, the well-known reaction limits, which have previously been investigated for premixed flames, but not for partially premixed flames, may exhibit a different behavior in the two reaction zones and warrants further investigation. In addition, H_2 –air PPFs can be expected to be more strongly influenced by Soret effects than other flames, as discussed later.

The objective of the present investigation is to examine the effect of pressure on the structure of counterflow hydrogen/air PPFs, and the existence of reaction limits in these flames. The counterflow configuration is considered because it represents both numerically and experimentally an ideal tool to study aerodynamic effects at various pressures. This configuration also has a well-defined velocity gradient and the governing equations can be reduced to a two-point boundary value problem that can be numerically simulated in one dimension. Thus, the counterflow configuration is well suited for performing a fundamental investigation of (1) the effect of pressure on the global and detailed chemical structure in the two reaction zones, (2) the interaction between the two reaction zones at different pressures, (3) the relevance of reaction limits for H_2 /air mixtures in the context of PPFs, and (4) the thermal diffusion (Soret) effect on the flame structure and reaction limits.

2. Physical–numerical model

The physical model considers a PPF in a counterflow configuration. The flame is established by igniting the fuel–air mixture formed by two opposing jets, one containing a rich H_2 –air mixture and the other containing air. The flame structure can be controlled by independently varying the equivalence ratio (ϕ) for a fixed global strain rate, a_s . The global strain rate

Table 1
Available experimental data for hydrogen flames

Configuration	Pressure (atm)	Strain rate (s^{-1})	Fuel composition	Reference
Counterflow nonpremixed flames	1	133	20% H ₂ /80% N ₂	Brown et al. [42]
		125	50% H ₂ /50% N ₂	
		100	100% H ₂	
Counterflow nonpremixed flames	1	100	30% H ₂ /70% N ₂	Rortveit et al. [11]
		100	35% H ₂ /65% N ₂	
		100	40% H ₂ /60% N ₂	
		100	45% H ₂ /55% N ₂	
		100	40% H ₂ /60% He	
		100	50% H ₂ /50% He	
Counterflow nonpremixed flames (strained induced extinction)	1	< 5670	14–100% H ₂ /air	Pellett et al. [43]
Outwardly propagating spherical flames	0.35–4.0	Ka < 1	H ₂ /O ₂ /N ₂ ($\phi = 0.45$ –4.0)	Aung et al. [24]
Outwardly propagating spherical flames	1	Ka < 0.4	H ₂ /air ($\phi = 0.45$ –4.0)	Aung et al. [44]
Outwardly propagating spherical flames	0.3–3.0	Ka < 0.5	H ₂ /O ₂ /(air, He or Ar) ($\phi = 0.6$ –4.5)	Kwon and Faeth [25]
Outwardly propagating spherical flames	1, 3, 5, 10, 15, 20	–	H ₂ /O ₂ /He ($\phi = 0.5$ –3.5)	Tse et al. [26]
Partially premixed flames	1	100	30% H ₂ /5.5% O ₂ /64.5% N ₂ ($\phi = 0.9$)	Rortveit et al. [11]
		100	35% H ₂ /5.5% O ₂ /59.5% N ₂ ($\phi = 1.0$)	
		100	40% H ₂ /5.5% O ₂ /54.5% N ₂ ($\phi = 1.2$)	
		100	35% H ₂ /4.5% O ₂ /60.5% N ₂ ($\phi = 1.0$)	
		100	35% H ₂ /6.0% O ₂ /59.0% N ₂ ($\phi = 1.0$)	
Counterflow nonpremixed ignition	4	300	9% H ₂ /91% N ₂ ($T_{\text{air}} = 1002$ K)	Fotache et al. [27]
Counterflow premixed ignition	0.6–7	216	H ₂ /air ($\phi = 0.236$)	Zheng and Law [31]

is characterized by the relation $a_s = (2|v_o|/L) \cdot \{1 + |v_f| \sqrt{\rho_f}/|v_o| \sqrt{\rho_o}\}$ [20], where L denotes the separation distance between the two jets, v_o the oxidizer jet inlet velocity, v_f the fuel jet inlet velocity, and ρ_f and ρ_o are the mixture densities in the fuel and oxidizer streams, respectively. The inlet velocities of the fuel and oxidizer streams are obtained by matching the momenta of the two streams for a given a_s . The ef-

fect of radiation is included, by using an optically thin radiation model.

Simulations of H₂–air PPFs, established at a given ϕ and a_s , are performed using the OPPDIF [21] code in the CHEMKIN package [22]. The distance between the two nozzles is 1.27 cm. The temperatures of the fuel and oxidizer nozzles are set at 300 K. The grid independence of the results was achieved by control-

ling the values of the GRAD and CURV parameters, both of which were set at 0.1, using adaptive regridding in order to resolve the structures of both the premixed and nonpremixed reaction zones. This required the number of grid points to be 250 for the lowest pressure case. As pressure is increased, the thickness of both the premixed and nonpremixed reaction zones decreases, and a satisfactory resolution of their structures for the highest pressure case required 1050 grid points. In order to examine the existence of reaction limits and transition between them, a PPF established at $\phi = 6.0$ was investigated by increasing the pressure from 1 to 40 atm for $a_s = 236 \text{ s}^{-1}$. A relatively high equivalence ratio was considered so that the transition between the reaction limits for H_2/air PPFs could be analyzed using a relatively moderate pressure range (1–40 atm). The strain rate of 236 s^{-1} is selected so that the fuel stream velocity (125.2 cm/s) at the nozzle exit is higher than the unstretched laminar flame speed at atmospheric pressure and $\phi = 6.0$. This avoids flashback for the range of pressures considered in this investigation since the fuel inlet velocity used is higher than the highest flame speed in this pressure range.

3. Results and discussion

3.1. Validation

The reaction mechanism used for our simulation was developed by Mueller et al. [23], which evolved from Yetter et al. [28] and Kim et al. [29] mechanisms, and was primarily aimed to reproduce more accurate results at higher pressure. It includes 19 reversible reactions and 8 reacting species. The mechanism has been previously validated at elevated pressures using experimental data for variable pressure flow reactors [23], freely propagating flames [24–26], and nonpremixed flames [27]. Fig. 1 presents a comparison of predicted and measured flame speeds versus fuel equivalence ratio at different pressures, while Fig. 2 presents the computed and measured flame speeds versus pressure at two different equivalence ratios. The PREMIX [35] and CHEMKIN [22] packages were used to predict the freely propagating flame speed. The comparison includes the measurements of Aung et al. [24], Kwon and Faeth [25] and Tse et al. [26], while the predictions are based on the Mueller et al. [23] and the GRI-Mech 3.0 [30] mechanisms. The latter is an optimized detailed reaction mechanism for methane–air mixtures and involves 325 elementary reactions with 53 species. The hydrogen submechanism included within GRI-Mech 3.0 has 20 reactions and 8 noninert species. The flame speeds were also computed using the Yetter et al. [28], and Kim et al. [29] mechanisms, but were not

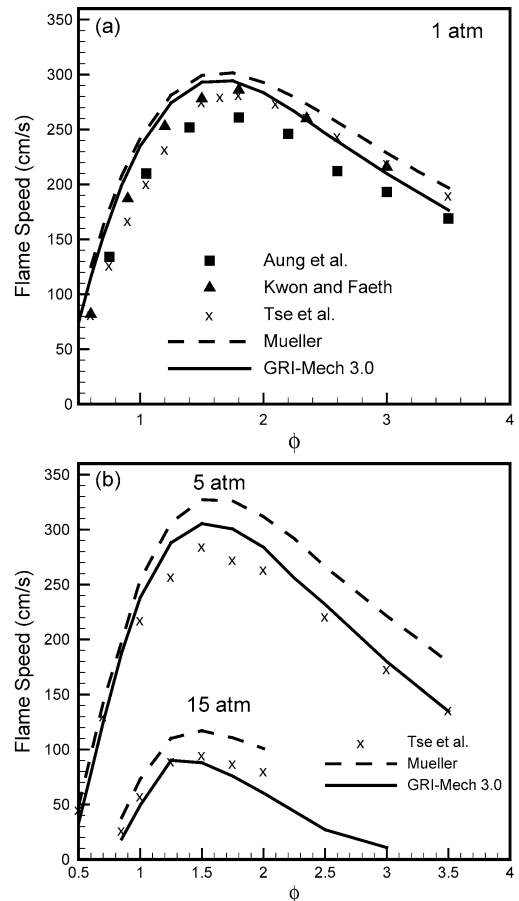


Fig. 1. Measured and predicted unstretched laminar flame speeds as a function of ϕ for (a) H_2/air flames at 1 atm, and (b) $\text{H}_2/\text{O}_2/\text{He}$ flames at 5 atm, where $\text{O}_2/(\text{O}_2 + \text{He}) = 0.125$, and at 15 atm, where $\text{O}_2/(\text{O}_2 + \text{He}) = 0.080$. Measurements are from Aung et al. [24], Kwon and Faeth [25], and Tse et al. [26]. Predictions are based on Mueller et al. [23] and GRI-Mech 3.0 [30] mechanisms.

included in the comparison because those were significantly less accurate than those obtained using the Mueller et al. [23] mechanism.

As indicated in Figs. 1 and 2, the Mueller et al. [23] mechanism is able to reproduce qualitatively the trend of the experimental data better than GRI-Mech 3.0 [30]. Although the latter mechanism exhibits better agreement with measurements at 1 and 5 atm (cf. Fig. 1), it overestimates flame speeds at low pressure and underestimates at higher pressures. Moreover, as indicated in Fig. 2, it becomes increasingly less accurate compared to the Mueller et al. [23] mechanism at higher pressures. Thus, the Mueller et al. mechanism [23] is found to be the most accurate for reproducing the effect of pressure on the flame speed, as well as the well-known reaction limits for H_2 –air mixtures, as discussed in the following.

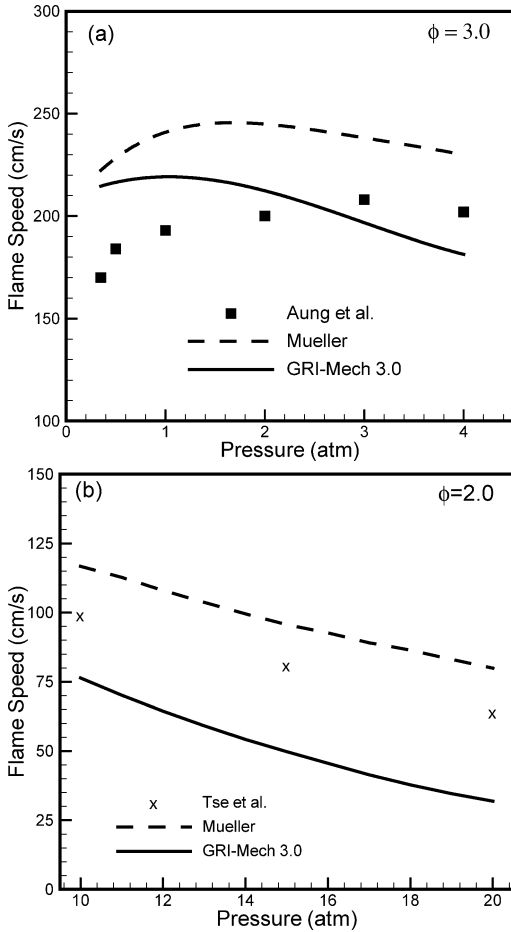


Fig. 2. Measured and predicted unstretched laminar flame speeds as a function of pressure for (a) H_2/air flames at $\phi = 3.0$, and (b) $\text{H}_2/\text{O}_2/\text{He}$ flames at $\phi = 2.0$, where $\text{O}_2/(\text{O}_2 + \text{He}) = 0.080$. Measurements are from Aung et al. [24] and Tse et al. [26]. Predictions are based on Mueller et al. [23] and GRI-Mech 3.0 [30] mechanisms.

3.2. Reaction limits for H_2/air mixtures

For H_2/air mixtures, it is important for a mechanism not only to predict the flame speed and structure, but also to reproduce the well-known reaction limits² [18]. Christiansen et al. [18] have shown the existence of three reaction limits for freely propagating H_2/air flames at $\phi = 7.0$ by plotting the mass-burning rate as a function of pressure. Recently, Zheng and Law [31] determined the temperatures of inert jets that ignited counterflowing lean premixed hydrogen/air jets

² Reaction limits refer to the stages of chain-branching and chain-terminating reactions that control the characteristics of a flame, while ignition limits refer to the different chain reactions that control autoignition.

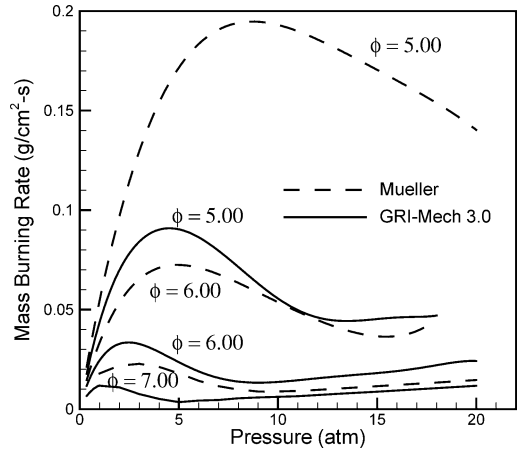


Fig. 3. Predicted mass-burning rate as a function of pressure at three different equivalence ratios. Predictions are based on Mueller et al. [23] and GRI-Mech 3.0 [30] mechanisms.

in the range 0.6–7 atm and $\phi = 0.236$. They were able to experimentally find a fourth ignition limit and even simulate a fifth such limit. Therefore, for a more comprehensive validation of the Mueller et al. [23] mechanism we have computed the mass-burning rate as a function of pressure for rich H_2 -air flames. Only the first three reaction limits are sought, since a very large pressure range is required to observe the other two limits.

Fig. 3 presents the mass-burning rate as a function of pressure for fuel-rich flames. The Soret effect is included in these simulations, since it is found to affect transition between the reaction limits, as discussed later. The maximum and minimum burning rates correspond to the transitions between first and second reaction limits, and second and third limits, respectively. The results show that the locations of both the local maximum and minimum mass-burning rates shift toward higher pressures as ϕ decreases in accord with the numerical investigation of Christiansen et al. [18]. The quantitative differences with the results of Christiansen et al. [18] are attributed to the modification of reaction (R9) in Mueller et al. [23] from its predecessor [29] through the change in the low-pressure rate constant, $k_{9,0}^{\text{N}_2}$. The effective reaction rate constant, k_9 , is now determined by the Troe fit [32,33] instead of the Lindemann–Hinshelwood fit [34] used in Kim et al. [29], which was the mechanism used by Christiansen et al. [18] with $F_c^{\text{N}_2} = 0.5$. As a result, the new effective pressure-dependent reaction coefficient $k_{9,\text{eff}}^{\text{N}_2}$ yields very good agreement with the second reaction limit. Moreover, Briones and Aggarwal [19] have shown that under atmospheric conditions the Mueller et al. [23] mechanism is more accurate than that proposed by Kim et al. [29]. There-

fore, the Mueller et al. [23] mechanism is used in this investigation.

3.3. Soret effect on the reaction limits

We have previously characterized the flame structure of a partially premixed flame at one atmosphere, and the effects of ϕ and a_s on that structure [19]. However, since many practical applications operate at high pressures, the influence of pressure on flame structure is an important consideration. Previous investigators have employed different criteria to identify the location of the rich premixed zone, such as the local maxima of the heat release rate [36], temperature gradient [37], and of certain species' concentration profiles [38]. The nonpremixed zone has been previously defined by the location of the maximum temperature [37]. However, the location of the maximum heat release rate on the oxidizer side is close to that of the peak temperature. Therefore, we employ the local peaks in the heat release rates to identify the rich premixed and nonpremixed zones on the fuel and oxidizer sides, respectively.

The Soret effect, which can be important when molecular and atomic hydrogen are present, is considered. Previous investigations [17] have shown that the Soret effect enhances the diffusion of H and H₂ into the reaction zone, increasing the extinction strain rate. This effect is nonnegligible when the temperature difference between fresh fuel and the reaction zone is large [39]. We expect it to influence the reactions on the rich side, which vary with pressure.

In order to characterize the Soret effect for H₂/air PPFs, we computed these flames for the base case ($\phi = 6.0$ and $a_s = 236 \text{ s}^{-1}$) at different pressures. Fig. 4a presents the computed temperatures with the Soret effect (\dot{T}_{Soret}) and without it (\dot{T}) at the location of the maximum heat release rate in the rich premixed zone as a function of pressure. The crossover temperature, which represents the temperature at transition between the reaction limits (T_{cross}), is also plotted in this figure. The crossover temperature is obtained by balancing the chain-branching reactions with the three-body recombination reaction with O₂ (i.e., $2k_1 = k_9[M]$). Transitions between the first and the second, and the second and the third reaction limits are indicated by the intersections of both \dot{T}_{Soret} and \dot{T} with T_{cross} , and shown by the numbers 1 and 2, respectively.

The Soret effect causes H₂ and H atoms to diffuse from low-temperature regions to high-temperature regions, with the net effect that it decreases the concentrations of these species in the rich premixed zone. This decreases the heat release rate and temperature in this zone, as indicated in Figs. 4b and 4c, which show the profiles of heat release rate, temperature,

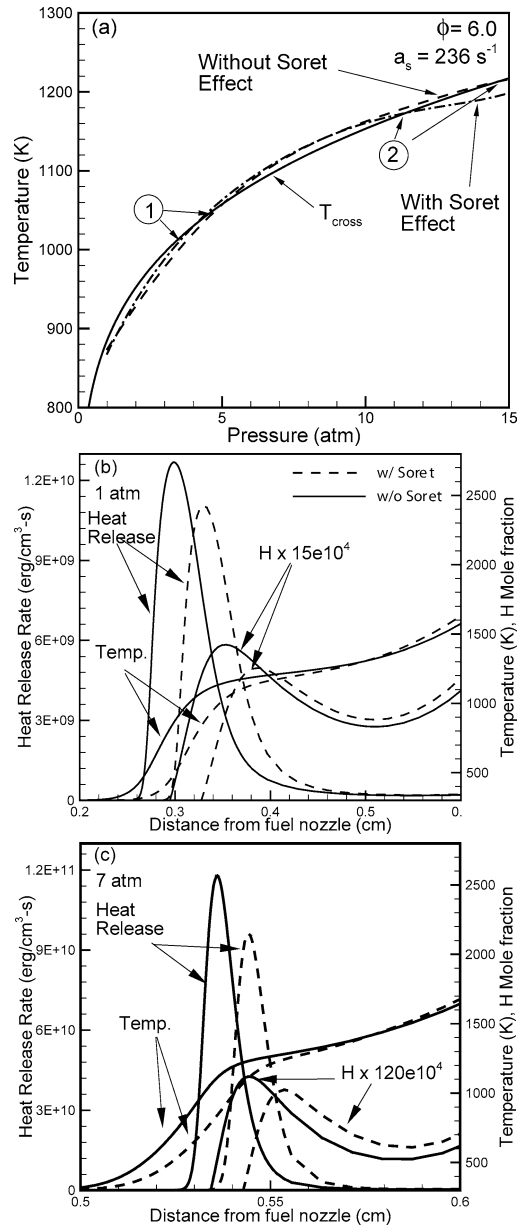


Fig. 4. Temperature at the location of maximum heat release rate, computed with and without the Soret effect, plotted as a function of pressure for a H₂–air PPF discussed in the context of Fig. 5. The crossover temperature is also shown. Numbers (1) and (2) represent transition from the first to the second limit, and from the second to the third limit, respectively. Profiles of heat release rate, temperature, and H-atom mole fraction computed with and without Soret effect at 1 atm (b) and 7 atm (c) are also shown.

and H-atom mole fraction for 1 and 7 atm. As a consequence, the flame speed is decreased, which moves the premixed zone downstream, as indicated by the shift in the peak values of the heat release rates when

Soret effect is included. In addition, as the temperature in the premixed zone decreases, it lowers the rate of reaction (R1) compared to that of (R9) due to the temperature-sensitive nature of (R1). Thus, the Soret effect shifts the transition between the first and the second reaction limits to a lower pressure; i.e., \dot{T}_{Soret} intersects T_{cross} at a $p \approx 4$ atm while \dot{T} intersects T_{cross} at ≈ 5 atm, as indicated in Fig. 4a. It is also noteworthy that, although the flame is stretched, intersection “1” (≈ 4 atm for the case with Soret effect) also corresponds to the local maximum of the mass burning rate, which is the transition between the first and the second reaction limits, for an unstretched premixed flame at $\phi = 6.0$ (shown in Fig. 3). Figs. 4b and 4c also indicate that with increasing pressure, the Soret effect becomes increasingly weaker, which is indicated by the decrease in the downstream shift of the peak heat release rate at higher pressure.

Transition from the second to the third reaction limit is characterized by a decrease in HO_2 and increase in the H_2O_2 concentrations. Our results indicate that as pressure increases, the decrease of HO_2 and increase of H_2O_2 concentrations are more pronounced with Soret effect included compared to that without Soret effect. This induces transition between the second to the third reaction limit to occur at a lower pressure, i.e., \dot{T}_{Soret} and \dot{T} cross T_{cross} at ≈ 11.5 and 14.5 atm, respectively, as indicated in Fig. 4a.

Fig. 3 shows that the minimum mass-burning rate occurs at ≈ 15.5 atm, again implying that the premixed reaction limits are not significantly affected by stretch. This might not be true at higher stretch rates since our flame here is only weakly stretched ($a_s = 236 \text{ s}^{-1}$). Moreover, the effect of stretch on the structure of the rich premixed zone may be less significant regardless of the pressure. For instance, our recent investigation of atmospheric counterflow H_2 -air PPFs shows that the rich premixed zone is less sensitive to stretching than the nonpremixed zone [19]. Results in Figs. 3 and 4 also demonstrate that the thermal structures of a premixed flame and the rich premixed zone of a PPF are influenced differently by the Soret effect, due to its influence on the computed reaction limits.

3.4. Effects of pressure on the PPF structure

In order to characterize pressure effects on H_2 -air PPFs, simulations were performed for the base case ($\phi = 6.0$ and $a_s = 236 \text{ s}^{-1}$) for a pressure range of 1–40 atm. The first set of results focuses on the relevance of the three reaction limits, as defined by the two intersections of \dot{T}_{Soret} and T_{cross} in Fig. 4, for these flames. Fig. 5 presents the (a) heat release rate, (b) temperature, and (c) velocity profiles for H_2 -air

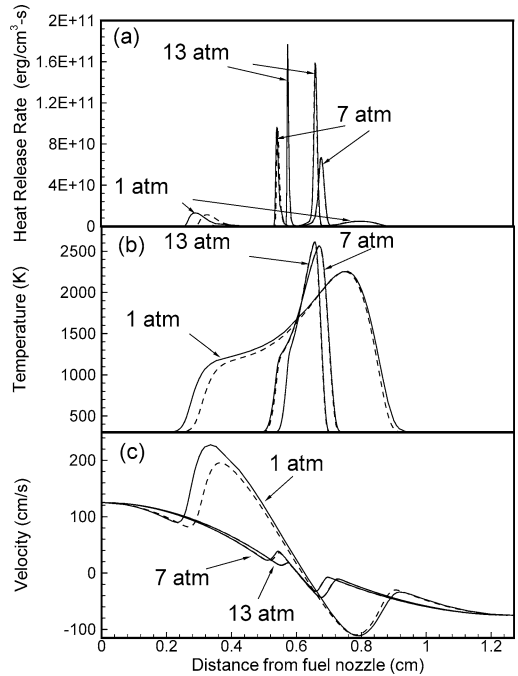


Fig. 5. Predicted heat release rate (a), temperature (b), and velocity profiles (c) for H_2 -air PPF established at $\phi = 6.0$ and at fixed $a_s = 236 \text{ s}^{-1}$ for 1, 7, and 13 atm. Predictions are based on the Mueller et al. [23] mechanism. Results are shown with and without (broken lines) radiation effect.

PPFs established at $\phi = 6.0$ and $a_s = 236 \text{ s}^{-1}$ at three different pressures. At low pressures ($p = 1$ atm), a H_2 -air PPF is characterized by two distinct reaction zones, namely a rich premixed zone on the fuel side and a nonpremixed zone on the oxidizer side. Detailed structures of the two reaction zones and interactions between them for $p = 1$ atm have been discussed by Briones and Aggarwal [19].

As pressure is increased, the separation distance between the two reaction zones decreases (cf. Fig. 5a). This is due to two effects. First as pressure increases, the flame speed associated with the rich premixed zone decreases, which stabilizes the rich premixed zone further downstream. This is clearly indicated by the velocity profiles presented in Fig. 5c. The second effect is due to the reduced mass diffusivity at high pressure, which decreases the transport of H atoms and unburnt hydrogen from the rich premixed zone to the nonpremixed zone and, thereby, moves the nonpremixed zone closer to the rich premixed zone. Results also indicate that the flame topology becomes relatively insensitive to pressure at higher pressures. As indicated by both the heat release rate and temperature profiles, as pressure is increased from 1 to 7 atm, the separation distance between the two reaction zones, as measured by the two heat release rate

peaks, decreases significantly, from 4.67 to 1.32 mm. However, as pressure is increased from 7 to 13 atm, and then from 13 to 40 atm, the separation distance only decreases from 1.32 to 0.85 mm, and then from 0.85 to 0.45 mm (cf. Figs. 5 and 15), respectively. Furthermore, the heat release rate profiles indicate that as pressure increases, the maximum heat release rates in both the rich premixed and nonpremixed reaction zones increase monotonically, indicating an increase in the global reaction rate. The increase in the heat release rate with pressure can mainly be attributed to reactions (R9), which is pressure sensitive and exothermic, and (R3), which produces H_2O . For the pressure range indicated in Fig. 5, the maximum heat release rate occurs in the rich premixed zone. However, at higher pressures, the heat release rate in the nonpremixed zone exceeds that in the rich premixed zone (cf. Fig. 14). It is also important to note that at higher pressures, while the heat release rate profiles exhibit a double-flame structure (i.e., a flame with two reaction zones), the temperature profiles indicate a nearly merged flame structure (cf. Fig. 5).

Another important observation from Fig. 5 is that radiation has a relatively small effect on the predicted flame structure. While its effect on the nonpremixed zone is negligible regardless of pressure, it is more noticeable on the rich premixed zone at atmospheric pressure. Although temperature is higher as pressure increases, thermal radiation becomes progressively less important since it is inherently a volumetric phenomenon. As discussed above, the spatial separation between the two reaction zones decreases significantly at higher pressures. In addition, the thickness of both the rich premixed and nonpremixed zones decreases as pressure is increased. For example, the thickness of the rich premixed zone decreases from 0.40 to 0.07 mm, while that of the nonpremixed zone decreases from 1.0 to 0.4 mm, as pressure is increased from 1 to 7 atm. Therefore, the effect of radiation on the PPF structure becomes negligible at higher pressures.

Liñán [40] noted that the width of the mixing layer scales as $(\rho \cdot a_s)^{-1/2}$ indicating that this width is inversely proportional to $p^{1/2}$. Sun et al. [36] conducted an extensive theoretical and computational investigation on the dynamics of weakly stretched flames. They determined that the flame thickness of H_2 –air premixed flames decreases with increasing pressure. Moreover, the peak temperature, which occurs in the nonpremixed zone, increases with increasing pressure. This implies that while the variations in ϕ and a_s mostly influence the rich premixed and nonpremixed reaction zone, respectively [19], pressure variations influence both reaction zones.

Briones and Aggarwal [19] reported that as ϕ or a_s increases the spatial separation between the two

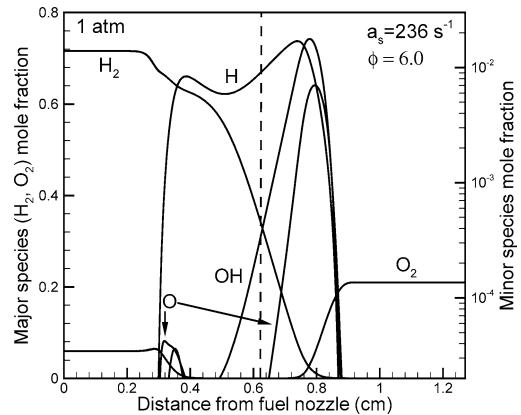


Fig. 6. Major (H_2 , O_2) and minor (H , OH , and O) species mole fraction profiles for the first reaction limit discussed in the context of Fig. 5. Location of the stagnation plane is indicated by the broken line.

reaction zones decreases, enhancing the thermochemical and fluid dynamic interactions between the two zones. There is a critical value at which the two reaction zones merge. Further increase in ϕ at a fixed a_s leads to a nonpremixed flame, while that in a_s leads to flame extinction. The merging of the two reaction zones caused by increasing ϕ or a_s is related to the flame speed associated with the rich premixed zone. This zone moves toward the stagnation plane when ϕ or a_s are increased in order to maintain a balance between the local flame speed and the flow velocity. Fig. 5c presents the velocity profiles for the counterflow PPFs at different pressures. The minimum axial velocity just ahead of the rich premixed zone decreases with increasing pressure. This is the stretched flame speed relative to the unburned gases and can be used to obtain the stretch-free flame speed relative to the unburned gases (s_{fl}^0). The effect of strain on the flame is expected to be progressively reduced by continuously decreasing the inlet velocities at the fuel nozzles. In the limit of vanishing local strain rate, k , the stretched flame speed should degenerate to the laminar flame speed [41]. In addition, the stretched flame speed is observed to decrease with pressure. Previous computational and experimental investigations [24–26,36] have reported a similar flame speed behavior with pressure. Understanding flame speed variations with pressure is crucial, since these changes have been recognized as a mechanism for merging the binary PPF structure into a single flame structure.

Fig. 6 presents the major and minor species for the PPF established at 1 atm. Both the H_2 and H mole fraction profiles indicate the separation between the two reaction zones. The fuel is partially consumed in the rich premixed zone, with the remaining fuel being transported to the nonpremixed zone. Briones and

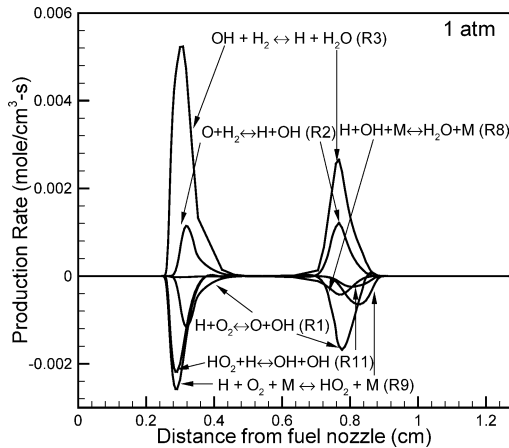


Fig. 7. Production/consumption rate profiles of hydrogen radicals within the first reaction limit discussed in the context of Fig. 5.

Aggarwal [19] observed that for a PPF established $\phi = 3.0$ and $p = 1$ atm, there is production of molecular hydrogen between the two reaction zones due to recombination of H radicals through $H + H + M \rightarrow H_2 + M$ (R5). This recombination is significantly reduced for the present case due to much higher ϕ , which increases the amount of unburned hydrogen in the rich premixed zone.

In order to examine the relevance of reaction limits, Fig. 7 presents the production/consumption rates of H atoms for the PPF at 1 atm. The maximum consumption of H atoms occurs through (R9) in the rich premixed zone and through (R1) in the nonpremixed zone. In both the reaction zones, (R1) and (R9) do not directly compete for H atoms. While (R9) has larger rates at lower temperatures, the rate of (R1) is more significant at higher temperatures. H-atom consumption through (R1) and production through (R2) are almost of the same magnitude (and at approximately the same location) in the rich premixed zone. The net effect of these two reactions is to produce OH, which is consumed through (R3). On the other hand, H-atom consumption in the nonpremixed zone through (R1) increases due to its temperature sensitivity. Here, its rate exceeds that of (R2) and is significantly larger than that of (R9), demonstrating that the nonpremixed zone is dominated by chain-branching reactions which characterize the first reaction limit. The consumption of H atoms occurs through (R9) at low temperatures in the rich premixed zone and through (R1) at high temperatures in the nonpremixed zone. Christiansen et al. [18] also found that for a rich premixed flame the reaction rate of (R9) is higher than that of (R1), but the flame is still dominated by the net chain-branching process (corresponding to the first limit).

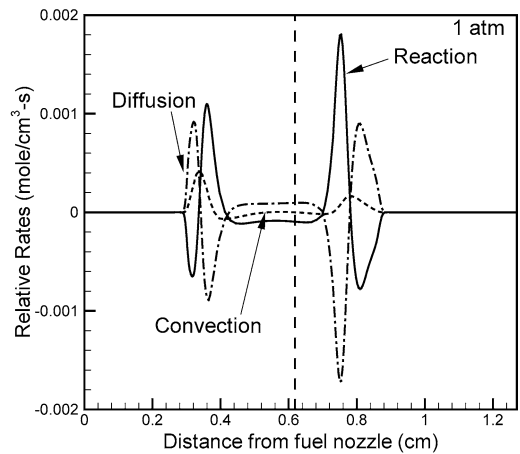


Fig. 8. Comparison of the relative rates of hydrogen radical production/consumption, and mass transport due to diffusion and convection within the first reaction limit for the PPF discussed in the context of Fig. 5. Location of the stagnation plane is indicated by the broken line.

Fig. 8 presents the relative rates of total chemical reaction and mass transport through diffusion and convection of H atoms for the PPF discussed in context of Fig. 7. It shows that H radical losses by diffusion are of the same order of magnitude as that of individual chemical production in both reaction zones (cf. Figs. 7 and 8). Previous investigations on ignition limits of H_2 -air nonpremixed flames [15] have identified diffusion as the major reason behind H radical losses within the first reaction limit. In fact, in the nonpremixed zone the H radicals exhibit a broad concentration profile (cf. Fig. 6), which indicates that H radicals are lost through diffusion from this zone (cf. Fig. 8).

Fig. 4a shows that the second reaction limit (in the rich premixed zone) lies between 4 and 11.5 atm. In order to examine this transition, Fig. 9 presents the flame structure in terms of appropriate species profiles at a pressure of 7 atm. Although the molecular hydrogen mole fraction profile is similar to that of the single-stage flame, the change in its slope indicates the existence of two reaction zones that are relatively close to each other. This is also indicated by the two peaks in the H-radical mole fraction profile. However, the O and OH radicals no longer show a peak in the rich premixed zone. This is because at this pressure, the rate of (R9) is substantially larger than that of (R1) in the rich premixed zone, while in the nonpremixed zone the rate of (R1) dominates (cf. Fig. 10). Moreover, as indicated in Fig. 10, while reactions (R1) and (R9) are in direct competition for H atoms at this pressure, they are not competing directly for H atoms at atmospheric pressure due to the shift in the locations of their reaction rate peaks (cf.

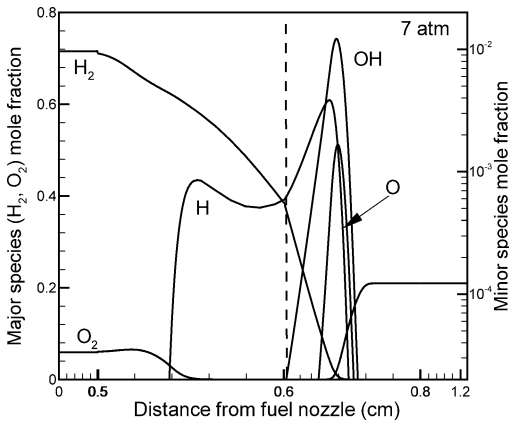


Fig. 9. Major (H_2 , O_2) and minor (H, OH, and O) species mole fraction profiles for the second reaction limit discussed in the context of Fig. 5. Location of the stagnation plane is indicated by the broken line.

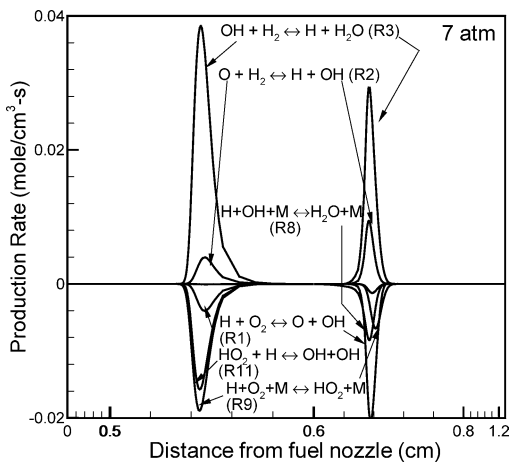


Fig. 10. Production/consumption rate profiles of hydrogen radicals within the second reaction limit discussed in the context of Fig. 5.

Fig. 7). This is an important result because it shows that although the rich premixed zone is now dominated by the chain-terminating reaction (R9), or the second reaction limit, the nonpremixed zone is still dominated by chain-branching reactions (R1), (R2), and (R3), or the first reaction limit.

Kreutz and Law [15] investigated the ignition behavior of H_2 /air mixtures, and observed that transition between the first and the second reaction limits is also associated with a significant drop in the diffusive loss of H radicals from the reaction zone. For the PPF at 1 atm, Figs. 7 and 8 indicate that the rate of H-radical diffusive loss is comparable to its individual production/consumption rates in the rich premixed zone. However, for the PPF at 7 atm, the H-radical diffusive loss in the rich premixed zone becomes negligible

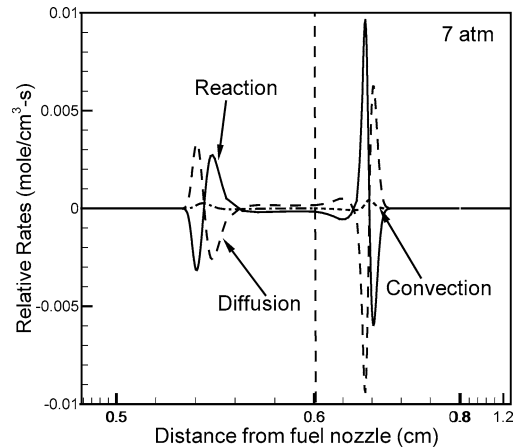


Fig. 11. Comparison of the relative rates of hydrogen radical production/consumption, and mass transport due to diffusion and convection within the second reaction limit for the PPF discussed in the context of Fig. 5. Location of the stagnation plane is indicated by the broken line.

comparable to its individual production/consumption rates, as indicated in Figs. 10 and 11. In addition, in the first limit, the net effect of (R1) and (R2) is to produce OH that is consumed through (R3). The temperature-sensitive reaction (R2) is almost invariant in both reaction zones at 1 atm (Fig. 6). However, at elevated pressures ($p = 7$ atm) the rate of (R2) in the nonpremixed zone is larger than in the rich premixed zone due to the higher concentrations of O and H_2 (Fig. 10). This suggests that chain-branching reactions continue to be dominant in the nonpremixed zone (first limit) until very high pressures are applied.

The third reaction limit (of the premixed zone) occurs at a pressure above 11.5 atm, as indicated in Fig. 4a. In order to analyze this transition, the flame structure in terms of appropriate species profiles at a pressure of 13 atm is presented in Fig. 12. Although the hydrogen profile is similar to that of a single-stage flame, the H-radical mole fraction profile exhibits two peaks, indicating the existence of two reaction zones. A major difference between the second and third reaction limits is due to the fact that HO_2 and H_2O_2 concentrations become significant in the third reaction limit. This indicates that production of HO_2 through (R9) and OH through reaction (R11) becomes significant. Therefore, OH must be consumed through (R3) at the same rate as it is produced. Intuitively, production of H_2O_2 must be occurring through reaction $2\text{HO}_2 \leftrightarrow \text{H}_2\text{O}_2 + \text{O}_2$ (R14), as has been identified by Christiansen et al. [18]. In the rich premixed zone, the dominant reactions peak nearly at the same location (Fig. 13). The net effect of (R1) and (R2) is almost the same as at lower pressures. However, the mixing layer in the nonpremixed zone narrows so that

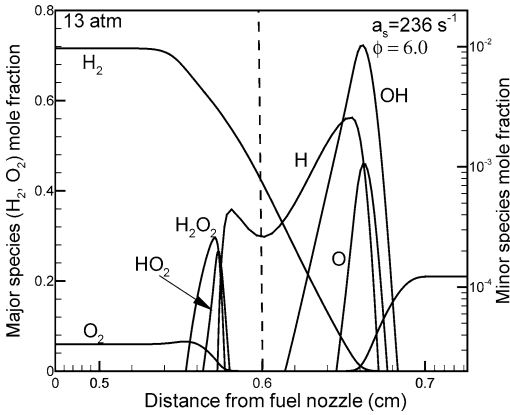


Fig. 12. Major (H_2 , O_2) and minor (H , OH , O , HO_2 , and H_2O_2) species mole fraction profiles for the third reaction limit discussed in the context of Fig. 5. Location of the stagnation plane is indicated by the broken line.

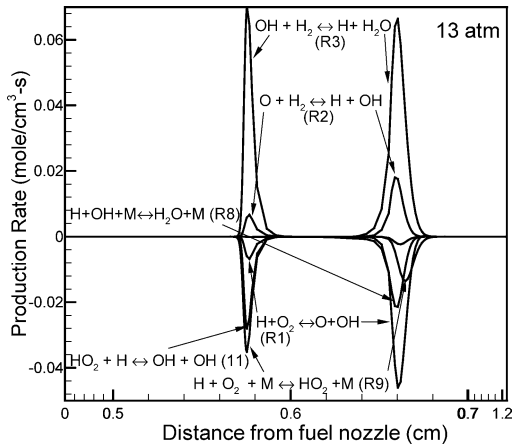


Fig. 13. Production/consumption rate profiles of hydrogen radicals within the third reaction limit discussed in the context of Fig. 5.

the locations where (R9) and (R1) are important are relatively much closer. The consumption of H atoms by (R1) is significantly larger so that the nonpremixed zone is characterized by a behavior corresponding to the first reaction limit in which chain-branching dominates over chain termination. Although the diffusive losses of H atoms are no longer relevant in the rich premixed zone, they continue to be quite significant in the nonpremixed zone. This is illustrated by comparing the relative magnitude of the diffusive losses in Fig. 14 with that of H-atom individual reaction rates in Fig. 13. Diffusive losses of H atoms become progressively less important as pressure increases mainly due to the reduction on the thickness of the rich premixed zone caused by the progressively decreasing thermal diffusivity.

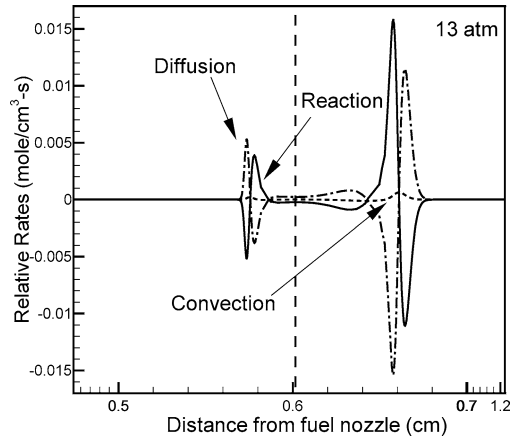


Fig. 14. Comparison of the relative rates of hydrogen radical production/consumption, and mass transport due to diffusion and convection within the third reaction limit for the PPF discussed in the context of Fig. 5. Location of the stagnation plane is indicated by the broken line.

An important implication from the above result is that a counterflow H_2 -air PPF can exploit the advantages of containing two reaction zones that are dominated by different types of chain reactions, one dominated by chain termination and the other dominated by chain branching. This suggests that the structure of a counterflow H_2 -air PPF under certain pressure conditions can be indicative to variations in both the fuel side equivalence ratio and the strain rate. For instance, variations of ϕ and a_s mostly influence the rich premixed and nonpremixed reaction zone, respectively. For stretch-free rich H_2 -air premixed flames, extinction equivalence ratios decrease for the first and second reaction limits and then increase toward the third limit [18]. For diluted H_2 -air nonpremixed flames, the extinction strain rates increase with pressure in the first limit, decrease in the second limit, and increase in the third limit [17]. In a counterflow H_2 -air PPF, the present results indicate that the premixed zone may be dominated by H-O_2 terminating reactions with additional HO_2 chain branching (pertinent to the third reaction limit), whereas the nonpremixed zone at the same pressure may be dominated by H-O_2 -branching reactions (relevant to the first limit). Therefore, such a flame should be strong enough to withstand variations in premixedness and aerodynamic straining.

By comparing Figs. 7, 10, and 13 it becomes clear that there is an additional difference in the manner in which pressure affects the two reaction zones. As the pressure is increased, the reaction rates of (R11) and (R8) increase in the rich premixed and nonpremixed zones, respectively. Since (R9) produces substantial amounts of HO_2 in the rich premixed zone, chain propagation through (R11) plays an important role in the transition between reaction limits in the pre-

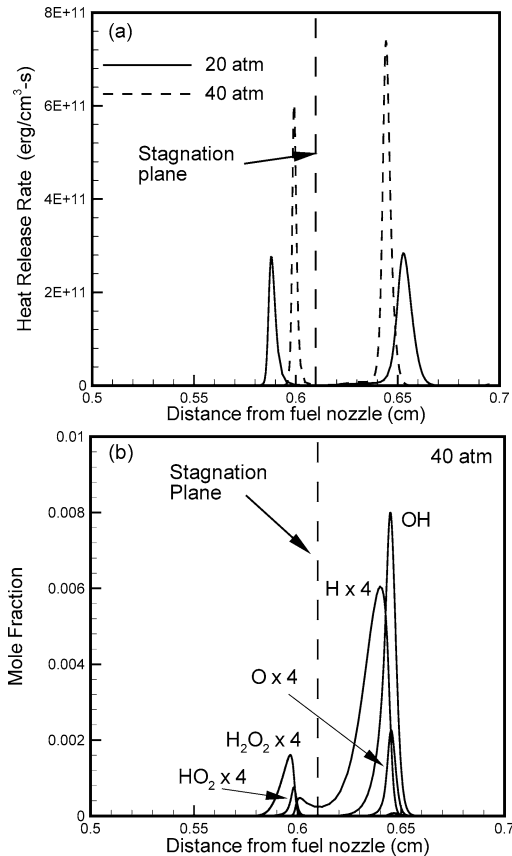


Fig. 15. Predicted heat release rate profiles at 20 and 40 atm (a), and intermediate species profiles (i.e., H, OH, O, HO₂, and H₂O₂) at 40 atm (b) for a H₂-air PPF established at $\phi = 6.0$ and at fixed $a_s = 236 \text{ s}^{-1}$. Results are shown with radiation effect.

mixed zone. On the other hand, (R11) is less important in the nonpremixed zone due to smaller amounts of HO₂ because this zone is dominated by H-O₂ chain-branching reactions. However, the reaction rate of (R8) is important in this zone.

In order to examine the flame structure and interaction between the two reaction zones at higher pressures, we present results for PPFs simulated at $p = 20$ and 40 atm. The heat release rate profiles for $p = 20$ and 40 atm are shown in Fig. 15a, and some appropriate species mole fraction profiles for $p = 40$ are shown in Fig. 15b. The heat release rate profiles indicate that even at relatively high pressures, the PPF structure is characterized by the existence of two distinct reaction zones. Moreover, the separation distance between the reaction zones becomes relatively insensitive to pressure; i.e., the two reaction zones do not merge even at very high pressures. This is because the flame speed associated with the rich premixed zone becomes nearly independent of pressure, reaching a value of $\sim 2.5 \text{ cm/s}$ in the high-pressure limit.

The nonpremixed reaction zone moves upstream, although only slightly, as pressure is increased from 20 to 40 atm, which is due to the reduced mass diffusivity at high pressures. Other species and dominant reaction rate profiles (not shown) also indicated that the qualitative structure of the PPF does not change significantly, as pressure is increased from 20 to 40 atm, although the thicknesses of the two reaction zones and the distance between them decrease. This also implies that the rich premixed zone and nonpremixed zone continue to be dominated by the third and first reaction limits, respectively, at high pressures.

4. Conclusions

We have investigated H₂-air partially premixed flames at high pressure in a counterflow configuration. Based on an extensive evaluation of the various hydrogen oxidation mechanisms, the Mueller et al. [23] mechanism is found to be the most suitable for our simulations. The mechanism satisfactorily predicts not only the variation of flame speed with pressure, but also the well-known reaction limits that are characteristic of H₂-air flames. The effect of pressure on the detailed structure of H₂-air PPFs has been characterized. Important observations are:

1. Similar to hydrocarbon fuel PPFs, the H₂-air PPF structure is characterized by two spatially distinct reaction zones. However, unlike hydrocarbon/air PPFs, the fuel is only partially consumed in the rich premixed zone with the remaining fuel being consumed in the nonpremixed zone. Another difference between the hydrogen and hydrocarbon fuel PPFs is that for the former, the nonpremixed zone is characterized by the H₂ oxidation chemistry, while for the latter it is characterized by the H₂ and CO oxidation chemistry.

2. As pressure increases, the thickness of each reaction zone decreases while the heat release rate in each zone increases. More importantly, the spatial separation between the two reaction zones decreases, which can be attributed to the effect of pressure on (i) flame speed associated with the rich premixed zone that decreases with pressure and, thereby, moves this zone downstream so as to maintain a balance between the local flame speed and the flow velocity, and (ii) mass diffusivity that decreases with pressure and, thus, moves the nonpremixed zone upstream (toward the fuel nozzle). Thus, the PPF structure can also be controlled by pressure, besides equivalence ratio and strain rate. At higher pressures, however, the effect of pressure on the flame structure is significantly reduced since the flame speed becomes nearly independent of pressure, and the flame maintains its twin-flame structure even at very high pressures.

3. The reaction limits, which have previously been examined in the context of ignition and combustion characteristics of H₂–air mixtures, have been investigated for H₂–air PPFs. Three reaction limits have been identified. The first reaction limit is characterized by the dominance of chain-branching reaction (R1), $H + O_2 \leftrightarrow OH + O$, compared to chain termination reaction (R9), $H + O_2 + M \leftrightarrow HO_2 + M$, and the diffusive losses of H atoms from the reaction zones being significant. The second limit is characterized by the dominance of (R9) over (R1), and the diffusive losses of H atoms being negligible. In the third limit, (R9) continues to be dominant producing significant amount of HO₂, which makes reactions (R11) ($HO_2 + H \leftrightarrow 2OH$) and (R14) ($HO_2 + HO_2 \leftrightarrow H_2O_2 + O_2$) important. Thus, the third limit is characterized by the increased concentrations of HO₂ and H₂O₂. The chemical structure of the nonpremixed zone is characterized by the first reaction limit in the entire range of pressure investigated ($p = 1$ to 40 atm). In contrast, the chemical structure of the rich premixed zone is characterized by the first reaction limit at low pressures, but undergoes transition to second limit at moderate pressures, and then to third limit at high pressure. The range of pressure for each reaction limit depends on the equivalence ratio (ϕ). As ϕ decreases or the level of partial premixing increases, transition between the reaction limits occurs at increasingly higher pressure. An important implication of this result is that depending on the pressure, a H₂–air PPF can take advantage of the fact that the two reaction zones can be dominated by different reaction limits or two different chain reactions, one dominated by chain termination and the other by chain branching. For example, for H₂–air PPFs established at $\phi = 6.0$ and $p = 13$ atm and higher, the rich premixed zone is dominated by the first limit, while the nonpremixed zone is dominated by the third limit.

4. The effects of radiation and thermal mass diffusion (Soret effect) on H₂–air PPFs have been characterized. The effect of radiation on the flame structure is found to be small, and becomes even less significant at higher pressures. The Soret effect causes a transition between the reaction limits to occur at lower pressures. However, the global flame structure is not significantly influenced by this effect.

5. A counterflow PPF provides a convenient way to determine the stretched and unstretched flame speeds as a function of pressure for a wider range of equivalence ratios, since the flammability limits are considerably extended with these flames.

Acknowledgments

This research was supported by the NSF Combustion and Plasma Systems Program for which Dr. Far-

ley Fisher has been the Program Director. Our work has been significantly enhanced through many discussions with Professor S.D. Tse, who also provided experimental data for flame speeds.

References

- [1] F.F. Flynn, R.P. Durrett, G.L. Hunter, A.O. zur Loye, O.C. Akinyemi, J.E. Dec, C.K. Westbrook, Diesel combustion: an integrated view combining laser diagnostics, chemical kinetics, and empirical validation, Paper 99-01-0509, SAE, 1999.
- [2] B.J. Lee, S.H. Chung, *Combust. Flame* 109 (1/2) (1997) 163–172.
- [3] L. Vervisch, *Proc. Combust. Inst.* 28 (2000) 11–24.
- [4] D.C. Haworth, R.J. Blint, B. Cuenot, T.J. Poinot, *Combust. Flame* 121 (3) (2000) 395–417.
- [5] J.W. Heffel, *Int. J. Hydrogen Energy* 28 (8) (2003) 901–908.
- [6] D.M. Kabat, J.W. Heffel, *Int. J. Hydrogen Energy* 27 (10) (2002) 1093–1102.
- [7] J.W. Heffel, *Int. J. Hydrogen Energy* 28 (11) (2003) 1285–1292.
- [8] M.A.S. Al-Baghdadi, *Renewable Energy* 28 (9) (2003) 1471–1478.
- [9] A.R. Choudhuri, S.R. Gollahalli, *Int. J. Hydrogen Energy* 25 (5) (2000) 451–462.
- [10] M.S. Kumar, A. Ramesh, A.R. Nagalingam, *Int. J. Hydrogen Energy* 28 (10) (2003) 1143–1154.
- [11] G.J. Rortveit, J.E. Hustad, S.-C. Li, F.A. Williams, *Combust. Flame* 130 (1/2) (2002) 48–61.
- [12] H.G. Im, J.H. Chen, *Combust. Flame* 119 (4) (1999) 436–454.
- [13] H.G. Im, J.H. Chen, *Combust. Flame* 126 (1/2) (2001) 1384–1392.
- [14] B.T. Helenbrook, C.K. Law, *Proc. Combust. Inst.* 26 (1996) 815–822.
- [15] T.G. Kreutz, C.K. Law, *Combust. Flame* 104 (1/2) (1996) 157–175.
- [16] T.G. Kreutz, C.K. Law, *Combust. Flame* 114 (3/4) (1998) 436–456.
- [17] C.H. Sohn, S.H. Chung, *Combust. Flame* 121 (1/2) (2000) 288–300.
- [18] E.W. Christiansen, C.K. Law, C.J. Sung, *Combust. Flame* 124 (1/2) (2001) 35–49.
- [19] A. Briones, S.K. Aggarwal, *Int. J. Hydrogen Energy*, 2004, in press.
- [20] I.K. Puri, K. Seshadri, *Combust. Flame* 65 (2) (1986) 137–150.
- [21] A.E. Lutz, R.J. Kee, J.F. Grcar, F.M. Rupley, Report No. SAND96-8243, Sandia National Laboratories, 1996.
- [22] R.J. Kee, F.M. Rupley, E. Meeks, J.A. Miller, Report No. SAND96-8216, Sandia National Laboratories, 1996.
- [23] M.A. Mueller, T.J. Kim, R.A. Yetter, F.L. Dryer, *Int. J. Chem. Kinetics* 31 (2) (1998) 113–125.
- [24] K.T. Aung, M.I. Hassan, G.M. Faeth, *Combust. Flame* 112 (1/2) (1998) 1–15.
- [25] O.C. Kwon, G.M. Faeth, *Combust. Flame* 124 (4) (2001) 590–610.

- [26] S.D. Tse, D.L. Zhu, C.K. Law, *Proc. Combust. Inst.* 28 (2000) 1793–1800.
- [27] C.G. Fotache, C.J. Sung, C.J. Sun, C.K. Law, *Combust. Flame* 112 (3) (1998) 457–471.
- [28] R.A. Yetter, F.L. Dryer, H. Rabitz, *Combust. Sci. Technol.* 79 (1/3) (1991) 97–128.
- [29] T.J. Kim, R.A. Yetter, F.L. Dryer, *Proc. Combust. Inst.* 26 (1994) 759–766.
- [30] M. Frenklach, C.T. Bowman, G.P. Smith, W.C. Gardiner, World Wide Web location http://www.me.berkeley.edu/gri_mech/, Version 3.0, 1999.
- [31] X.L. Zheng, C.K. Law, *Combust. Flame* 136 (1/2) (2004) 168–179.
- [32] J. Troe, *Chem. Phys. Chem.* 83 (1979) 114.
- [33] J. Troe, *Ber. Bunsenges Physik. Chem.* 84 (1983) 829.
- [34] F. Lindemann, *Trans. Faraday Soc.* 17 (1922) 598.
- [35] R.J. Kee, J.F. Grcar, M.D. Smooke, J.A. Miller, E. Meeks, Report No. SAND85-8240, Sandia National Laboratories, 1985.
- [36] C.J. Sun, C.J. Sung, L. He, C.K. Law, *Combust. Flame* 118 (1/2) (1999) 108–128.
- [37] H.S. Xue, S.K. Aggarwal, *AIAA J.* 40 (11) (2002) 2289–2297.
- [38] M.A. Tanoff, M.D. Smooke, R.J. Osborne, T.M. Brown, R.W. Pitz, *Proc. Combust. Inst.* 26 (1996) 1121–1128.
- [39] G. Balakrishnan, M.D. Smooke, F.A. Williams, *Combust. Flame* 102 (3) (1995) 329–340.
- [40] A. Liñán, *Acta Astronaut.* 1 (7/8) (1974) 1007–1039.
- [41] C.K. Law, C.J. Sung, *Prog. Energ. Combust. Sci.* 26 (4/6) (2000) 459–505.
- [42] T.M. Brown, M.A. Tanoff, R.J. Osborne, R.W. Pitz, M.D. Smooke, *Combust. Sci. Technol.* 129 (1997) 71–88.
- [43] G.L. Pellett, K.M. Isaac, W.M. Humphreys Jr., L.R. Gartrell, W.L. Roberts, C.L. Dancy, G.B. Northam, *Combust. Flame* 112 (4) (1998) 575–592.
- [44] K.T. Aung, M.I. Hassan, G.M. Faeth, *Combust. Flame* 109 (1/2) (1997) 1–24.